

www.acsami.org Research Article

Tuning the Interfacial Properties of Fluorous Colloids Toward Ultrasound Programmable Bioactivity

Atip Lawanprasert, Alda Chau, Janna N. Sloand, Sean Hannifin, and Scott H. Medina*



Cite This: ACS Appl. Mater. Interfaces 2021, 13, 5989-5998

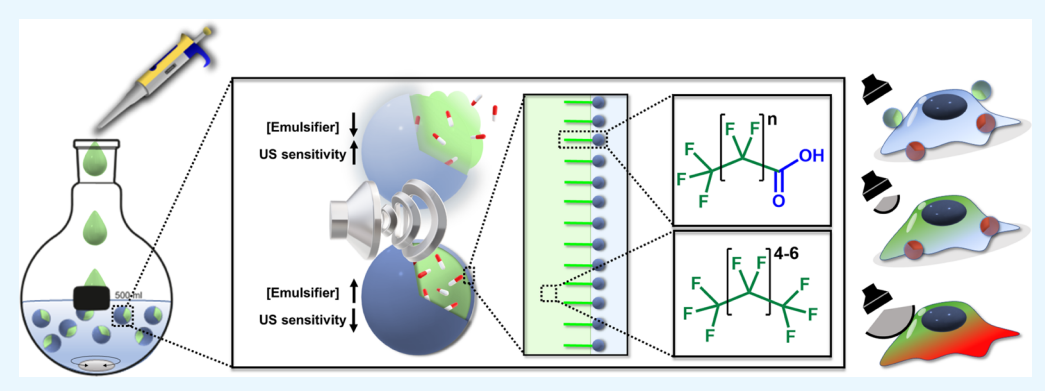


ACCESS





Supporting Information



ABSTRACT: Liquid-in-liquid emulsions are kinetically stable colloids that undergo liquid-to-gas phase transitions in response to thermal or acoustic stimuli. Perfluorocarbons (PFCs) are preferred species as their highly fluorinated nature imparts unique properties that are unparalleled by nonfluorinated counterparts. However, traditional methods to prepare PFC emulsions lack the ability to precisely tune the thermodynamic stability of the fluorous—water interphase and consequently control their vaporization behavior. Here, we report a privileged fluoroalkanoic acid that undergoes concentration-dependent assembly on the surfaces of fluorous droplets to modulate interfacial tension. This allows for the rational formulation of orthogonal PFC droplets that can be programmed to vaporize at specified ultrasound powers. We exploit this behavior in two exemplary biomedical settings by developing emulsions that aid ultrasound-mediated hemostasis and enable bioorthogonal delivery of molecular sensors to mammalian cells. Mechanistic insights gained from these studies can be generalized to tune the thermodynamic interfacial equilibria of PFC emulsions toward designing controllable tools for precision medicine.

KEYWORDS: emulsions, interfacial thermodynamics, ultrasound, spatiotemporal, drug delivery, fluorine

■ INTRODUCTION

Colloidal particles, including liposomes, nanospheres, and emulsions, are versatile biomaterial platforms upon which an array of chemical separation, biomedical imaging, and pharmaceutical technologies have been built. Among these, vaporizable liquid-in-liquid emulsions are a thermodynamically privileged class of particles with broad applications in multimodal imaging, energy storage, energy storage, and drug delivery. When controlled release is desired, emulsions are often prepared using an amphiphilic emulsifier that is rationally tuned in its physicochemical properties to control the rate of passive cargo release (i.e., diffusion) from the emulsified phase. Notable work by the Sletten Lab, for example, has yielded poly(2-oxazoline) surfactants that enable control over payload retention, with the added functionality of tuning emulsion size and surface chemistry for drug delivery purposes. 22,23

A practical alternative to passive cargo release is active release. Here, vaporization of the emulsion carrier in response to thermal, optical, or mechanical stimuli enables on-demand payload release. ^{19,24–34} Perfluorocarbon (PFC) solvents are well suited for these applications due to their strong intramolecular C–F bonds, which impart a biologically and chemically inert character while being sufficiently volatile to undergo liquid–gas phase transitions under physiologically compatible conditions. ^{33,35} The latter property has been exploited to control PFC droplet vaporization in response to changes in temperature²⁴ or exposure to light^{25–30} and ultrasound (US). ^{19,31–34} In the case of biomedical ultrasonics, acoustic vaporization of PFC droplets on a heterogeneous surface leads to the nucleation of a highly echogenic microbubble. ^{36–38} Collapse of this bubble potentiates the

Received: November 14, 2020 Accepted: January 21, 2021 Published: February 1, 2021





release of therapeutic cargo and, when paired with the echogenic response from bubble cavitation, enables spatio-temporal theragnostic utility.

Yet, adoption of US-sensitive emulsions has been slowed down by the need to empirically refine the emulsifier and PFC species for each specific therapeutic or diagnostic setting. This is because tuning the critical vaporization temperature of these particles, and thus their US responsiveness, requires balancing two interdependent elements—particle size and interfacial thermodynamics. This complexity has impeded the rational design of scalable PFC materials with programmable US activation thresholds. ^{39,40} If realized, such platforms could open new opportunities for multiplexed gene editing and drug delivery by creating uniformly sized droplets that can be orthogonally activated using different conditions of US. However, this is not yet achievable with traditional emulsions prepared from a single PFC species as they are intrinsically limited to a discrete continuum of US activation pressures. To resolve this hurdle, two or more PFCs with varying vaporization temperatures are combined to tailor the desired thermodynamic stability of the mixed system. Although this approach has been successfully applied in vitro and in vivo, 5,35,41,42 the use of multiple fluorous solvents increases the synthetic complexity of the carrier, requires empirical optimization of mixture ratios, and complicates the formulation of multiple bioactive cargoes into the combinatorial carrier. A more facile approach would be to develop a single molecular emulsifier that can tune the thermodynamic surface properties of chemically homogeneous, single-species PFC emulsions to precisely control their acoustic behavior without the need for complex mixtures.

Here, we report a privileged small-molecule fluoroamphiphile that undergoes templated assembly at fluorous—water interfaces to alter the kinetic stability of PFC droplets. This allows for precise tuning of emulsion surface tension, decoupled from particle size, to control the energy required to nucleate vaporization of the emulsified phase. Consequently, we can prepare emulsions from a single PFC species, which can be programmed in their response to various US stimuli. We demonstrate the utility of this strategy in two exemplary biomedical applications: US-assisted hemostasis and orthogonal, spatiotemporal release of bioactive cargoes.

MATERIALS AND METHODS

Materials. Perfluoropentanoic acid, perfluorononanoic acid (PFNA), perfluorotetradecanoic acid, perfluorooctadecanoic acid, and 1,1'-di-n-octadecyl-3,3,3',3'-tetramethylindocarbocyanine perchlorate (DiI) were purchased from Alfa Aesar (Haverhill, MA). Perfluoropropionic acid, perfluoroheptane (PFH_p), perfluorohexane (PFH_x), and perfluorooctane (PFO_c) were purchased from Oakwood Chemical (Estill, SC). Perfluorooctanoic acid was purchased from TCI Chemical (Portland, OR). Perfluoroundecanoic acid was purchased from Sigma-Aldrich (St. Louis, MO). 3,3'-Dioctadecyloxacarbocyanine (DiO) was purchased from Cayman Chemical (Ann Arbor, MI). ProLong Diamond Antifade Mountant with 4',6diamidino-2-phenylindole dihydrochloride (DAPI) was purchased from Invitrogen (Carlsbad, CA). Human umbilical vein endothelial cells (HUVECs) (ATCC PCS-100-010), vascular cell basal medium, and the Endothelial Growth Cell Kit-VEGF were purchased from ATCC (Manassas, VA). RPMI-1640 culture medium was purchased from Lonza (Basel, Switzerland). Fetal bovine serum (FBS), Lglutamine (L-Gln), trypsin, and phosphate-buffered saline (PBS) were purchased from Corning (Corning, NY). Gentamycin hydrochloride was ordered from VWR (Radnor, PA). Paraformaldehyde (PFA, 4%) was ordered from Chem Cruz (Dallas, TX). Thiozolyl blue

tetrazolium bromide (MTT) was obtained from Chem-Impex (Wood Dale, IL). Dimethyl sulfoxide (DMSO) was purchased from Thermo Fisher (Waltham, MA). The HUVEC cell line was gifted by Dr. Yong Wang's lab at Penn State, Department of Biomedical Engineering. The A549 cell line was provided by the National Cancer Institute (NCI).

Emulsifier Screening. A library of fluoroalkanoic acids, including pentaperfluoropropionic acid, perfluoropentanoic acid, perfluorooctanoic acid, perfluorononanoic acid (PFNA), perfluoroundecanoic acid, perfluorotetradecanoic acid, and perfluorooctadecanoic acid, was dissolved in perfluorohexane (PFH_x) at 25 mM. Emulsification was initiated by adding dropwise PFH_x containing each emulsifier to deionized (DI) water at a final volume ratio of 1:6 in a round-bottom flask with stirring at 1200 rpm for 1 h. Optical density measurements (OD₆₀₀) were performed via UV-vis spectrophotometry (Agilent Technologies; Santa Clara, CA) to evaluate the relative emulsification efficiency of each fluorochemical. Particle density (particles/mL) was calculated from OD_{600} measurements normalized to a standard curve prepared via particle counting (Figure S1). Particle counting was performed by diluting a PFO emulsion solution 1:1 in trypan blue, and the number of particles per area was calculated from images collected on a hemocytometer using ImageJ software.

PFC Emulsion Physicochemical Characterization. Interfacial tension measurements were performed via pendant drop using a ramé-hart Model 295 automated goniometer/tensiometer (Succasunna, NJ). PFNA was dissolved at 0–20 mM concentrations in PFH_x, PFH_p, or PFO_c. A flat-tip stainless steel 0.5 in. 28G needle (Hamilton; Reno, NV) was connected to a gas-tight glass syringe (1 mL) holding the PFNA-dissolved PFC solution. The needle was submerged ~5 mm into 1 mL of water in a 10 mm quartz cuvette, and then, PFNA-dissolved PFC droplets were manually dispensed into water to form a pendant drop. DROPimage Advanced software was used to capture pendant images and interpret droplet interfacial tension using Young's equation. Ten images and interfacial tension measurements (1 s⁻¹) per droplet were captured across six different droplets (n = 60).

Diameters of PFNA-stabilized emulsions were measured for each PFC solution at 2.5–30 mM concentrations of the emulsifier. Bright-field images of particle solutions were collected at 20× magnification using a Cytation 3 plate reader (BioTek; Winooski, VT). The diameter of each formulation was measured via ImageJ software.

Emulsion surface charge was measured by ζ -potential analysis of emulsions diluted 1:10 in water before addition to a disposable folded capillary cell (Malvern, DTS1070; Malvern, PA). Phase analysis light scattering (PALS)-assisted ζ -potential measurements were performed with three independent replicates at 25 or 40 °C temperatures, with 2 minutes of equilibration between measurements.

Thermal-Induced Emulsion Vaporization. Thermal phase change of PFC emulsions was measured for particles prepared from PFH_x, PFH_p, and PFO_c solvents and PFNA emulsifier concentrations of 2.5–30 mM. A representative sample of each prepared formulation was mounted on a glass slide and imaged at 20× magnification using a Cytation 3 plate reader at room temperature to capture the initial droplet morphology. The sample was heated at 1 $^{\circ}$ C/min, and images were taken as a function of time. $T_{\rm exp}$ was determined as the temperature at which droplet circumference exponentially increased.

Programming Acoustic Responsiveness of PFC Droplets. Acoustic activation of PFNA-stabilized PFH $_{\rm w}$ PFH $_{\rm p}$, PFO $_{\rm c}$ emulsions was measured by diluting particles in DI water before addition to a 96-well plate. Ultrasound was applied at a power of 0–3 W/cm 2 (30 s, 50% duty cycle) using a submerged 6 mm 1 MHz transducer (Nepagene, Chiba, Japan). After acoustic treatment, the sample solution was transferred into a clean well and the optical density (OD $_{600}$) was measured. The normalized particle density, indicating the fraction of undisrupted droplets, was calculated as follows

$$\text{norm. particle integrity} = \frac{OD_{600-treated} - OD_{600-background}}{OD_{600-initial} - OD_{600-background}}$$

To illustrate the change in acoustic response for each formulation, the effective power required for 50% droplet disruption (EP_{50}) was calculated from asymmetric curve fitting using GraphPad Prism 8 software.

Cell Culture. A549 cells were cultured in complete RPMI-1640 media containing 10% v/v FBS, 2 mM $_{\rm L}$ -Gln, and 0.05 mg/mL gentamycin hydrochloride. HUVEC cells were cultured in vascular cell basal medium supplemented with 5 ng/mL rhVEGF, 5 ng/mL rh EGF, 5 ng/mL rh FGF basic, 15 ng/mL rh IGF-1, 10 mM $_{\rm L}$ -glutamine, 0.75 U/mL heparin sulfate, 1 $_{\rm H}$ g/mL hydrocortisone hemisuccinate, 2% v/v FBS, and 50 $_{\rm H}$ g/mL ascorbic acid. All cells were cultured at 5% CO $_{\rm 2}$ and 37 °C.

Biocompatibility of PFNA-PFO Emulsions. The biocompatibility of PFNA-PFO_c emulsions toward HUVEC cells was assessed via the MTT assay. In a typical experiment, 5000 HUVEC cells/well were seeded into a 96-well plate and incubated overnight to adhere. The supernatant was then replaced with 100 μ L of treatment solution prepared by serially diluting PFNA-PFO_c emulsions in complete growth media to achieve concentrations between $OD_{600} = 0.0001$ $(10^2 \text{ particles/mL})$ and $OD_{600} = 1.0 (10^6 \text{ particles/mL})$. Blank growth media and growth media containing 20% DMSO were included as negative and positive controls, respectively. Treated cells were then insonated at 2.0 W/cm² for 30 s and left to incubate for an additional 24 h. The supernatant was then removed and replaced by 100 μ L of media containing 0.5 mg/mL MTT dye, followed by 3 h incubation to allow dye conversion. Cells were then lysed, and the formazan product was solubilized with the addition of 100 μ L of DMSO. The absorbance of the solution was read at 540 nm using a BioTek Cytation 3 microplate reader, and cell viability determined as

$$\text{\% viability} = \frac{\lambda_{\text{treatment}} - \lambda_{\text{positive}}}{\lambda_{\text{negative}} - \lambda_{\text{positive}}} \times 100\%$$

Hemolytic activity of PFNA-PFO_c emulsions was measured by first concentrating bovine red blood cells (RBCs) via centrifugation of whole blood at 600 rpm for 30 min. Pelleted RBCs were washed with hemolysis buffer (10 mM Tris, 150 mM NaCl, pH 7.4), repelleted at 3460 rpm for 10 min at 4 °C, and the RBC solution was diluted to a final concentration of 0.25% v/v in hemolysis buffer. The RBC stock (75 μ L) and an equivalent volume of 2× PFNA-PFO_c emulsion, formed using 20 mM or 30 mM PFNA emulsifier, in hemolysis buffer were mixed and then added into the 96-well plate. Blank buffer and 1% Triton X-100 in buffer were included as negative and positive controls, respectively. The hemolytic activity of activated PFNA-PFO emulsions was assessed by exposing the solution to 2.0 W/cm² US for 30 s. After 24 h incubation, plates were centrifuged at 4000 rpm for 10 min to pellet intact RBCs. The supernatant (100 μ L) was transferred to a clean 96-well plate before reading the absorbance at 415 nm using a BioTek Cytation 3 plate reader. Percentage hemolysis was calculated

%hemolysis =
$$\frac{\lambda_{\text{treatment}} - \lambda_{\text{negative}}}{\lambda_{\text{positive}} - \lambda_{\text{negative}}} \times 100\%$$

Coagulation Kinetics Assay. The clotting time assay was performed by first preparing a platelet-rich plasma (PRP) solution by centrifuging whole bovine blood at 600 rcf for 30 min at 4 °C. Then, 450 μ L of PRP and 5 μ L of PFNA-PFO_c emulsion solution in water were mixed to achieve a final concentration of 10⁵ particles/mL and added to a 24-well plate. For US-treated groups, a 6 mm 1 MHz transducer (Nepagene, Chiba, Japan) was submerged into the solution and insonated at 2 W/cm² for 30 s before initiating clotting. Coagulation was then initiated by adding 50 μ L of 0.1 M CaCl₂ solution to each well, and the clotting time was determined as the time postrecalcification when the solution became visually viscous. Normalized clotting time was calculated relative to PRP solutions left untreated with particles or US.

Platelet aggregation was measured by collecting bovine platelets from PRP via centrifugation at 800 rcf for 15 min at room temperature. The cell pellet was then resuspended in 1× PBS and

transferred to a microcentrifuge tube. In each tube, the PFNA-PFO $_{\rm c}$ emulsion was added to achieve 10^5 particles/mL. Acoustic activation was applied as described above for US-treated groups. An equal volume of water was added to a separate platelet suspension to serve as a negative control. After 15 min of incubation, the treated samples were collected and subjected to flow cytometry analysis. Platelet aggregation was quantified by measuring changes in aggregate size from front scattering (FSC) data.

US Delivery of Lipophilic Dyes. A stock concentration of 100 μ M DiI and DiO was prepared by dissolving the dyes in diethyl ether and chloroform, respectively. At the start of droplet emulsification, an aliquot of DiO solution was added to 20 mM PFNA-PFO_C particles in water to a final volume ratio of 1:7. The same procedure was used to prepare DiI-loaded 30 mM PFNA-PFO_c particles. The solutions were then stirred overnight to vaporize organic solvents. The emulsions were washed three times by successive iterations of emulsion sedimentation via gravity, supernatant removal, and addition of DI water. Emulsion formulations were diluted to the same particle density before experiments. Initial sequential activation experiments were performed by adding a 500 μ L volume of DiO-loaded (20 mM PFNA-PFO or DiI-loaded (30 mM PFNA-PFO emulsions to a four-well chamber slide. The mixtures were then subjected to US at 0, 0.4, and 3.0 $\ensuremath{W/cm^2}$ using a 50% duty cycle for 1.5 min. Confocal microscopy (FluoView FV1000; Olympus; Tokyo, Japan) was used to image the particles immediately after US activation, and the percentage of activated particles was determined by counting the number of intact particles normalized to the untreated control using

In vitro cargo delivery studies were performed by seeding 20,000 A549 cells/well in a four-well chambered slide, and cells were allowed to incubate at 37 °C overnight to adhere. The supernatant media was then replaced by 1 mL of complete growth media containing 10⁵ particles/mL of DiO-loaded (20 mM PFNA-PFO_c) or DiI-loaded (30 mM PFNA-PFO_c) emulsions. After 30 min incubation, US was applied at a power of 0, 0.1, 0.4, 1.0, and 2.0 W/cm² at 50% duty cycle for 30 s. Immediately after ultrasound treatment, cells were washed with PBS twice and fixed with 4% PFA. Slides were then mounted and stained with DAPI using ProLong Diamond Antifade Mountant. Cells were imaged using an FV1000 Olympus confocal microscope at multiple locations with respect to the acoustic probe. ImageJ software was used to measure the average fluorescent intensity of labeled cells.

Statistical Analysis. All values are reported as mean \pm standard error of mean (SEM) or standard deviation (SD), as indicated in the text. Statistical significance was determined using Student's *t*-test with $p \leq 0.05$ reported as statistically significant.

■ RESULTS AND DISCUSSION

Emulsifier Selection and Thermodynamic Surface **Properties.** Emulsifier discovery began by screening a library of perfluorocarboxylic acids with increasing organofluorine content (Figure 1). This class of perfluoroalkyls was selected based on their weak intermolecular interactions, which results from the low polarizability of fluorines, juxtaposed to the strong electronegatively of the fluorous tail that leads to a highly acidic carboxy hydrophile (p K_a range of -0.63 to -0.05). Together, these properties yield amphiphiles ideally positioned for assembly at water-fluorous interfaces (Figure 1A). Preparation of PFC emulsions using fluorous solvent perfluorohexane (C₆F₁₄, PFH_x) identified perfluorononanoic acid (PFNA; n = 7) as a lead candidate with clear superiority in forming stable colloids (Figure 1B). In contrast, addition or subtraction of 1-2 CF₂ groups yielded perfluorocarboxylic acids unable to form competent emulsions with PFH_x (see n =6 and 9 in Figure 1B). To our knowledge, the dependence of emulsion stability on the length of the fluoroalkyl tail has not been previously reported for perfluorocarboxylic acids. However, analogous side-chain-dependent changes in the

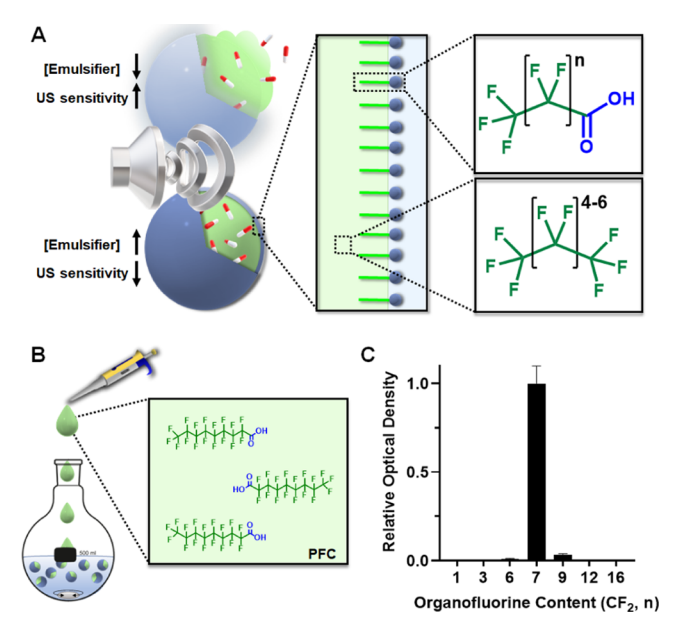


Figure 1. (A) Schematic of US-sensitive emulsions prepared from PFC droplets (green) stabilized via interfacial assembly of perfluorocarboxylic amphiphiles (blue). Tuning the concentration-dependent assembly of the emulsifier at the fluorous—water interphase enables control over the energy required for acoustic droplet vaporization and consequently allows US-programmable release of the bioactive cargo (red). (B) Diagram of emulsion synthesis via dropwise addition of the PFC solvent containing the fluoroamphiphile emulsifier to a stirred water solution. (C) Perfluorocarboxylic acid screen to identify fluoroamphiphiles capable of forming stable emulsions with PFH $_{xr}$ as determined by optical density measurements (OD $_{600}$). Results are displayed as a function of increasing organofluorine content (CF $_{21}$, n) of the tested emulsifier.

stability of hydrocarbon surfactant micelles have been observed. For example, studies employing mixtures of sodium dodecyl sulfate (SDS) and varying chain length alkyltrimethylammonium bromides (TABs) found that C₁₂TAB caused the greatest magnitude change in aqueous surface viscosity and tension and produced more stable micelles, relative to analogous C₈-C₁₀ and C₁₄-C₁₆ TAB formulations. ⁴³ This behavior was mechanistically explained by the optimal packing observed for C₁₂TAB at air-water interfaces during partition experiments. The authors suggest that mixtures of SDS and C₁₂TAB create complexes that possess amphiphilic properties optimized to avoid dissolution into either the hydrocarbon or aqueous bulk phases, and instead preferentially organize at the interphase. Extrapolating these results to our system suggests that PFNA possesses a unique counterbalance of polarity and fluorine content that makes it particularly well suited for templated assembly at fluorous-water interfaces.

Using the PFNA emulsifier, emulsions were prepared from three PFC solvents with increasing bulk vaporization temperatures, including PFH_x (bp = 57 °C), perfluoroheptane (PFH_p, bp = 81 °C), and perfluorooctane (PFO_c, bp = 104 °C). Emulsions prepared from each solvent using 2-20 mM PFNA yielded droplets approximately 5-8 μm in diameter (Figure 2A,B). Concentrations of PFNA > 20 mM resulted in a slight increase in the average emulsion diameter to $\sim 20 \mu m$ for PFH_v and PFH_p, while PFO_c remained consistent at a \sim 6 μ m particle size. Further evidence of this is shown in Figure 2C, which confirms that PFO_c emulsions prepared from 20 and 30 mM PFNA, two formulations prioritized in later biologic studies, possess a similar particle size-frequency distribution. This is important as we have previously shown that the energy required to vaporize PFC emulsions is interdependent on both particle size and interfacial surface tension.⁴⁴ Thus, we can use PFNA-PFO_c emulsion formulations to decouple droplet size from the acoustic response and therefore independently tune

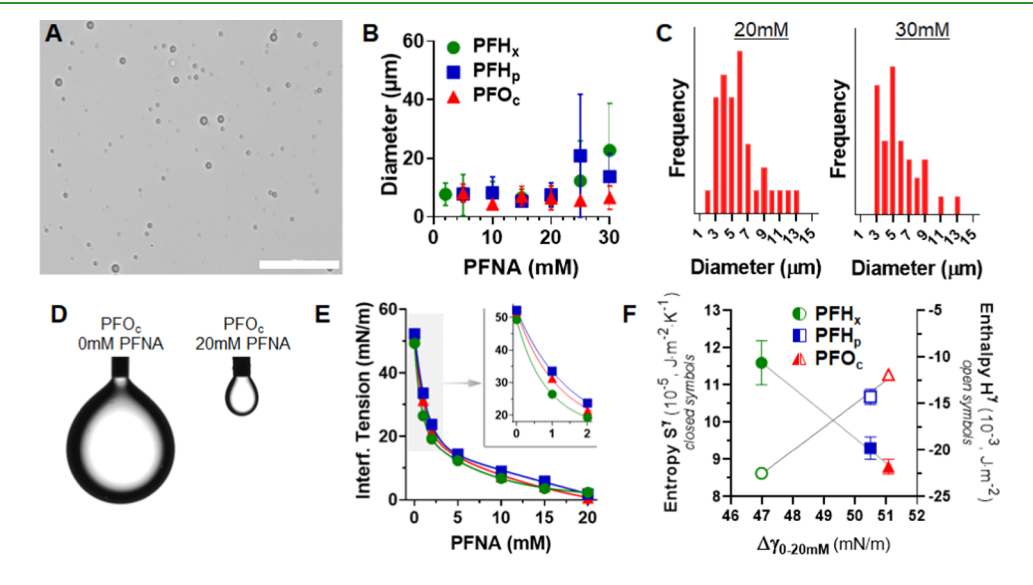


Figure 2. (A) Optical micrograph of 20 mM PFNA-stabilized PFH_x emulsions in water. Scale bar = 100 μm. (B) Mean emulsion diameter as a function of the PFC solvent and PFNA concentration, as measured from particle micrographs using ImageJ software ($n \ge 5$). (C) Frequency distribution plots of particle diameter for PFO_c emulsions prepared using 20 mM (left) or 30 mM (right) PFNA emulsifier. (D) Representative images of PFO_c pendant droplets containing 0 mM (left) or 20 mM (right) dissolved PFNA. (E) Interfacial tension of droplets prepared from PFH_x (green), PFH_p (blue), or PFO_c (red) as a function of the PFNA concentration. Inset: Differential interfacial tensions at low PFNA concentrations (0−2 mM). (F) Correlation between the magnitude change in interfacial tension for each PFC at 0 and 20 mM PFNA concentration ($\Delta \gamma_{0-20mM}$) relative to the surface entropy (S^γ, closed symbols) and enthalpy (H^γ, open symbols) of each solvent at room temperature. Reported values for S^γ and H^γ obtained from ref 45. Gray lines are included to guide the eye.

emulsion surface tension to precisely control their US vaporization threshold.

Next, we performed pendant drop assays to study the concentration-dependent influence of PFNA on the interfacial biophysics of PFC droplets in aqueous media. This technique measures the change in the PFC droplet curvature as a function of the solubilized PFNA concentration to calculate interfacial tension values (Figure 2D). All three PFCs tested showed a logarithmic decrease in interfacial tension with increasing concentration of dispersed PFNA at ambient (27 °C) conditions (Figure 2E). Interestingly, although all three PFCs possess a similar initial surface tension in the absence of PFNA (~51 mN/m), the magnitude change in interfacial tension at high concentrations of PFNA (20 mM) was generally found to follow the trend PFO_c > PFH_p > PFH_x. Plotting the magnitude change of interfacial tension for each PFC between 0 and 20 mM PFNA (Figure 2F, $\Delta \gamma_{0-20\text{mM}}$) indicates a linear correlation with reported surface entropy (S^{γ}) and enthalpy (H) values of the three corresponding PFC solvents at room temperature. 45 This suggests that PFNA's capacity to disrupt intermolecular interactions between PFC molecules, and thus alter droplet surface tension, is the greatest for fluorous solvents in which surface enthalpy is maximized relative to entropic contributions of interfacial free energy.

US-Programmable Vaporization of PFC Emulsions. PFNA's ability to modulate the intermolecular surface interactions of fluorous droplets should allow it to control the thermodynamic stability of PFC emulsions and, hence, the energy required for vaporization. To test this assertion, we first determined the critical temperature at which liquid-gas phase transitions (T_{exp}) occur for each PFNA-stabilized formulation (Figure 3A,B). PFH_x and PFO_c emulsions, both of which showed a significant reduction in surface tension following PFNA assembly (Figure 2E), became highly thermosensitive in the presence of the emulsifier. For example, the addition of 2.5 mM PFNA was sufficient to reduce the critical temperature of PFH_x and PFO_c to ~27 °C. Conversely, PFH_p emulsions were markedly less sensitive to destabilization by PFNA, reaching a similar vaporization temperature (27 °C) at a 10-fold higher concentration of PFNA (25 mM) relative to the other two PFCs tested. This observation can be explained, in part, by Laplace pressure, where the differential surface tension of PFH_n relative to the other tested PFCs at low PFNA concentrations (see Figure 2E, inset) shifts its kinetic equilibrium toward higher temperatures.

Another contributing factor to the observed thermal behavior may be the altered solubility of PFNA in the different PFC species employed. The vaporization temperature of volatile liquids is defined by intermolecular interactions between constituent molecules. Thus, it is possible that preferential solubilization of PFNA in PFH_x and PFO_c, relative to PFH_p, may increase the likelihood of disrupted intermolecular interactions in bulk solution to strongly drive the thermodynamic instability of these formulations.

Next, we measured the US power required to nucleate heterogeneous vaporization of the emulsions, as determined by a change in the solution optical density (OD_{600} , Figure S2). For these studies, we prioritized formulations prepared from 20 to 30 mM PFNA due to their high particle yield, as well as long-term stability against coalescence (Ostwald ripening) during storage. Figure 3C demonstrates that the acoustic energy required to vaporize PFC emulsions increased monotonically with PFNA concentration. Moreover, the

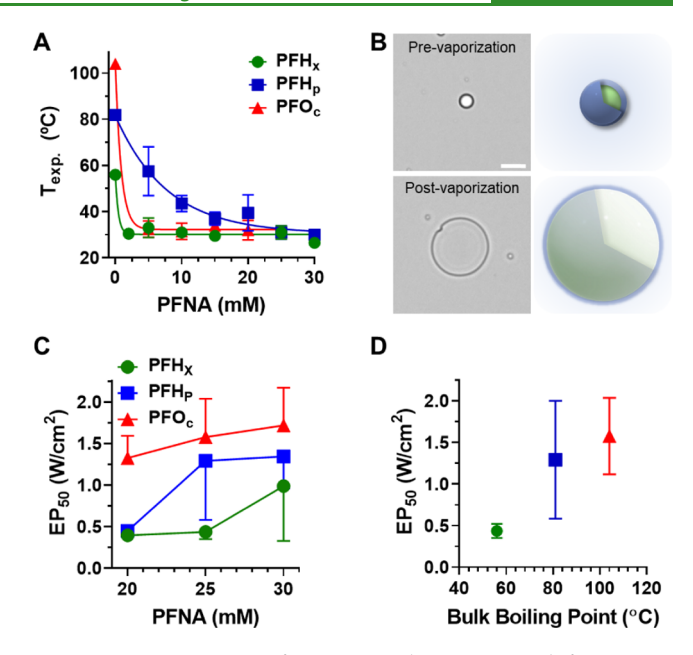


Figure 3. Vaporization of PFNA emulsions prepared from PFH_x (green), PFH_p (blue), or PFO_c (red) fluorous solvents. (A) Threshold temperature for expansion of PFC emulsions ($T_{\rm exp}$) as a function of the PFNA concentration. (B) Optical micrographs (left) and schematic images (right) of a PFNA-PFO_c droplet before (top) and after (bottom) vaporization to form an echogenic microbubble. Scale bar = 10 μ m. (C) Effective US power required to vaporize 50% of PFC emulsions (EP₅₀), plotted as a function of the fluorous solvent and PFNA concentration. (D) Relationship of effective US vaporization power and bulk solvent boiling point for PFC emulsions prepared at 25 mM PFNA.

effective US power required to vaporize 50% of the particles in solution (EP_{50}) scaled linearly with the vaporization temperature of each PFC for 25 and 30 mM PFNA formulations (Figures 3D and S3). These results diverge from the findings of our thermal vaporization studies (Figure 3A), where increasing PFNA concentration decreased the thermal stability of PFCs droplets. Results from our acoustic vaporization experiments (Figure 3C), instead, suggest the opposite correlation.

One possible explanation for this divergent biophysical behavior lies in the different methods (i.e., thermal versus mechanical) employed to initiate phase transition. Under US, droplets oscillate during compression and rarefaction (expansion) phases of the acoustic signal. If acoustic pressure causes the emulsion to oscillate out of equilibrium, defined as the Blake threshold, ⁴⁶ droplets undergo nonlinear expansion and grow in size. ^{47,48} Influx of dissolved oxygen into the expanding bubble increases its volume until it becomes unstable and violently collapses, a process termed inertial cavitation. During this process, it is possible that excess PFNA partitions to the interface to suppress the formation of a vapor embryo, thus stabilizing the expanding bubble surface and impeding the influx of dissolved oxygen that precedes inertial cavitation. In parallel to this effect, high concentrations of PFNA may also promote the fractionation and recondensation of vaporized droplets into small emulsions that, due to Laplace pressure, require increased acoustic energy to undergo the phase change. Supporting this assertion are zeta potential measurements performed before and after vaporization of PFO_c emulsions prepared at high (30 mM) and low (7.5 mM) PFNA concentrations (Figure S4). Results demonstrate that

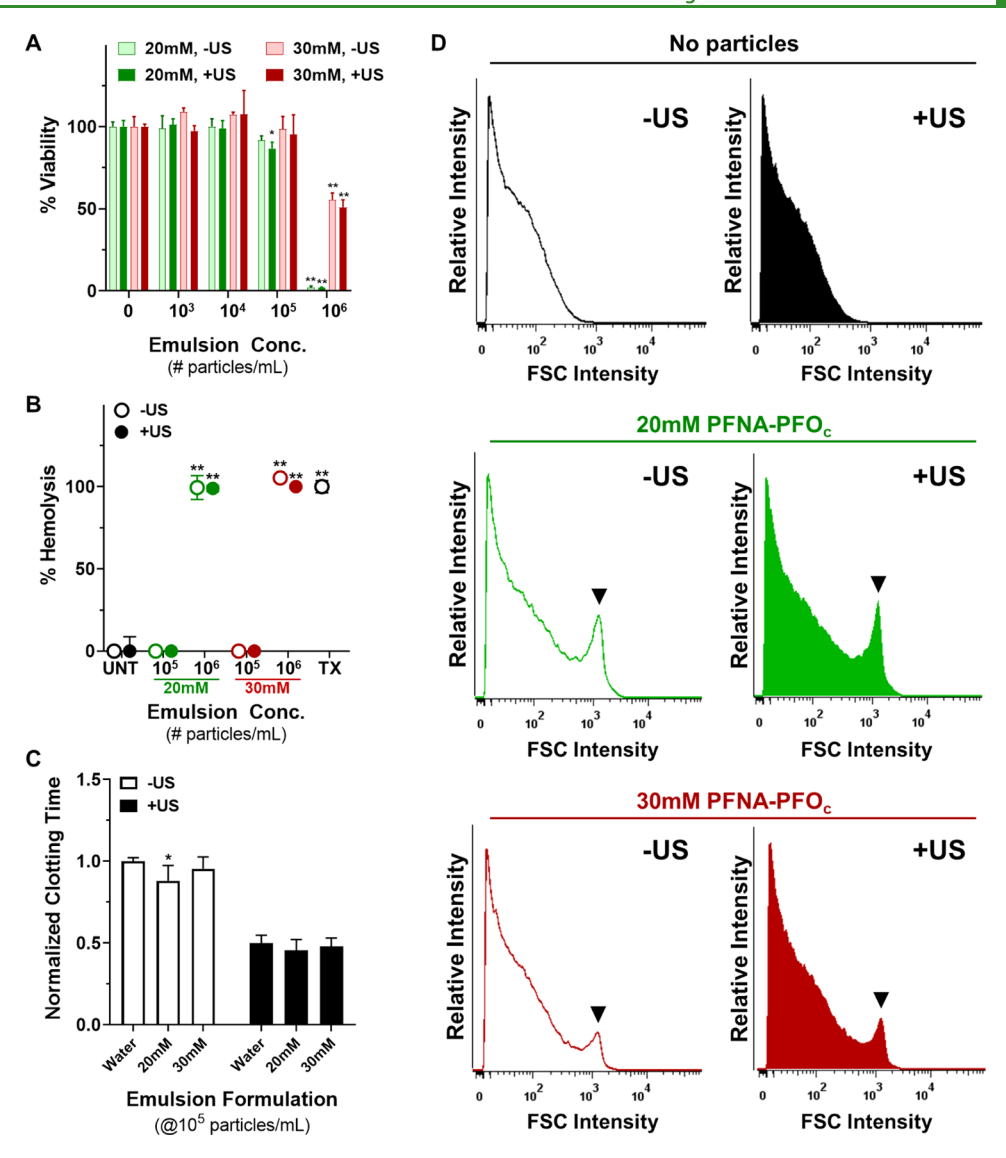


Figure 4. (A) HUVEC viability following 24 h incubation with increasing particle densities of 20 mM (green) or 30 mM (red) PFNA-PFO_c emulsions before (light color, -US) and after (dark color, +US) acoustic cavitation. (B) Percent hemolysis of bovine erythrocytes before (open circle, -US) and after (filled circle, +US) acoustic activation of 20 mM (green) or 30 mM (red) PFNA-PFO_c emulsions. Blank buffer (UNT) and 1% Triton X-100 (TX) solution were included as negative and positive controls, respectively. (C) Relative clotting time of recalcified platelet-rich plasma containing 20 or 30 mM PFNA-PFO_c emulsions (10^5 particles/mL) before and after US vaporization. Data are normalized to the clotting time of plasma mixed with a blank aliquot of water. For panels (A)-(C), statistical significance was determined relative to untreated controls using Student's *t*-test, with * indicating *p* < 0.05 and ** indicating *p* < 0.01. (D) Platelet aggregation following 15 min incubation of bovine platelets with 20 or 30 mM PFNA-PFO_c emulsions (10^5 particles/mL) before (-US) and after (+US) acoustic activation. Data are shown as the number of events (relative intensity) versus forward scattering (FSC) intensity. Black arrows indicate highly scattering platelet aggregates. US was applied to all experiments at 2 W/cm² and 50% duty cycle for 30 s.

after thermal vaporization only 30 mM PFNA-PFO $_{\rm c}$ emulsions produced a secondary, weakly anionic manifold of particles. Conversely, low PFNA formulations (7.5 mM) showed a reduction in the density of particles after vaporization at the original zeta potential of -55 mV, with no appearance of a secondary population. Although mechanistically disparate from our thermal vaporization studies, these findings cumulatively demonstrate that the acoustic power required to cavitate PFNA-stabilized emulsions can be readily controlled by modulating the amount of emulsifier that assembles at the fluorous—water interface.

Emulsion-Assisted Hemostasis and Orthogonal Biomolecule Delivery. Next, we performed separate *in vitro* studies designed to leverage the acoustoresponsive behavior of

PFNA-PFO_c emulsions for precision medicine applications. The first is to improve the efficiency of US-assisted blood coagulation for rapid hemostasis. Focused US has recently emerged as an attractive modality for noninvasive, or minimally invasive, thermal ablation to induce site-specific coagulation and control acute hemorrhage. However, the application of US to control bleeding in deep tissues often requires high acoustic intensities to overcome scattering by superficial tissues. Mechanical disruption of adjacent tissue by these high-intensity acoustic fields can lead to collateral organ trauma. Microbubble-enhanced US can overcome these off-target effects by inducing hemostasis at low acoustic intensities through the enhancement of ultrasonic local heating and by causing cavitation-mediated damage to the capillary endothe-

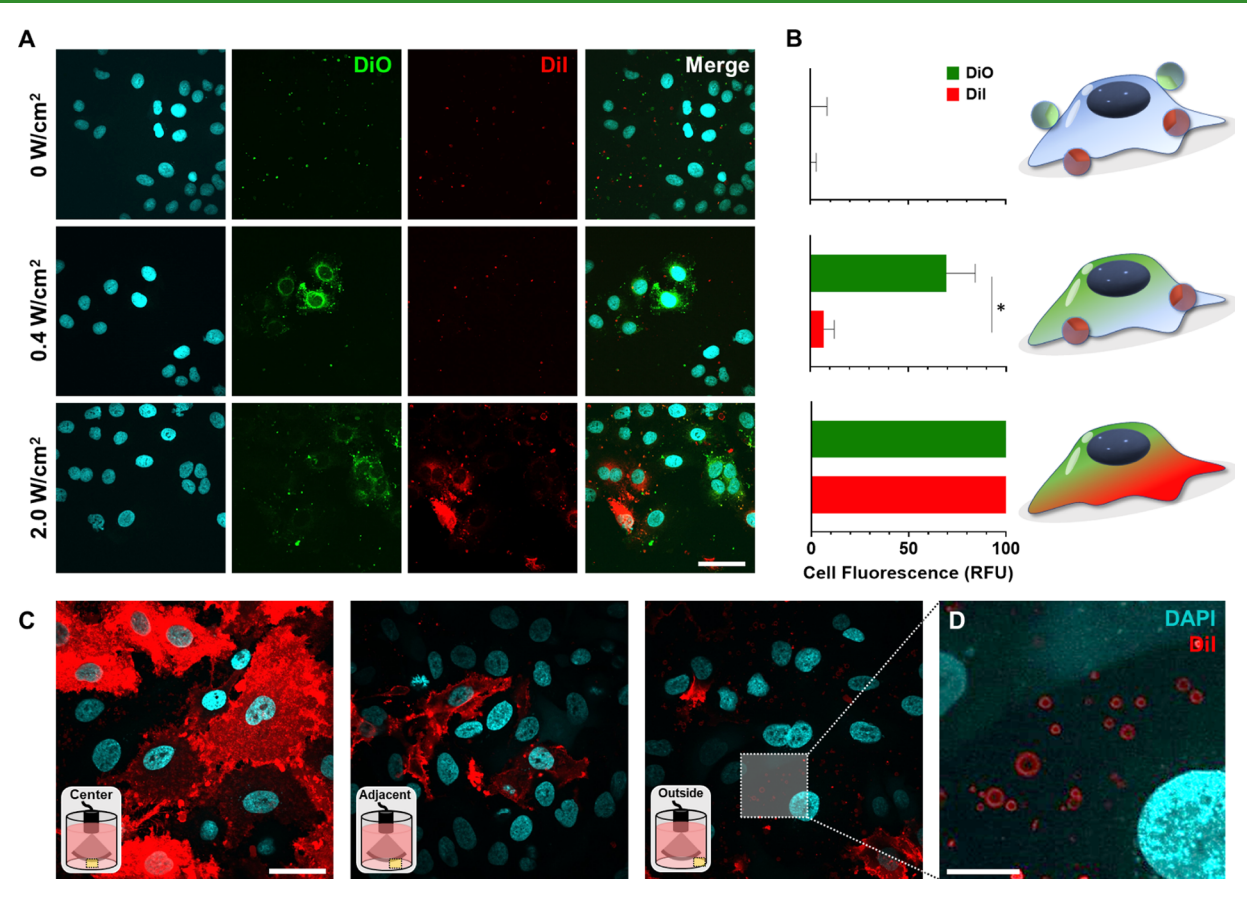


Figure 5. (A) Fluorescent confocal micrographs of human A549 cells cotreated with combinatorial PFO_c emulsions encapsulating DiO (20 mM PFNA; sensitive to low US power) or DiI (30 mM PFNA; sensitive to intermediate US power). Cells were either left uninsonated (0 W/cm²) or emulsions were differentially activated by an exogenous US pulse at low (0.4 W/cm²) or intermediate (2.0 W/cm²) power. Scale bar = 50 μm. (B) Left: Quantitation of cellular fluorescence (shown in relative fluorescence units, RFU) following sequential delivery of DiO (green) and DiI (red) at each US activation power. Right: Schematic of orthogonal particle activation and sequential dye delivery to cells. Statistical significance is determined using Student's *t*-test, with * indicating p < 0.05. (C) Fluorescent micrographs collected at different positions along the A549 cell monolayer following US activation of DiI-loaded PFNA-PFO_c emulsions. Images show cells in the center (left), adjacent to (middle), or outside (right) of the acoustic field generated by the US transducer (see the position schematic in the lower left of each image). Scale bar = 50 μm. (D) Magnified region of interest (white box in panel C) demonstrating that DiI-loaded PFNA-PFO_c emulsions (red) remain intact outside of the US acoustic field. Scale bar = 20 μm.

lium and erythrocytes. 52,53 With this in mind, we investigated the ability of PFNA-PFO emulsions to facilitate rapid coagulation in a low-intensity acoustic field. We hypothesized that the differential vaporization of 20 and 30 mM PFNAemulsified PFO droplets could be exploited to impart programmable control over the coagulation kinetics. Before initiating these experiments, we first tested the hemocompatibility of the two formulations in the absence and presence of the US trigger toward human endothelial cells and bovine erythrocytes. Cell viability assays confirmed that both pre- and postvaporized PFNA-PFO_c emulsions were well tolerated by human umbilical vein endothelial cells (HUVECs) up to concentrations of 10⁵ particles/mL (Figure 4A). At the highest tested particle concentration (10⁶ particles/mL), both PFNA-PFO_c formulations displayed toxicity that was independent of their US activation status, with greater cell killing observed for 20 mM PFNA-PFO_c emulsions (~95% cell death) relative to 30 mM formulations (~50% cell death). This differential cytotoxicity may be related to the thermodynamic stability of each formulation. Here, the decreased kinetic stability of 20 mM PFNA-PFO_c emulsions relative to 30 mM formulations (see Figure 3C) may make them more susceptible to disassembly in a lipophilic environment, like the cell

membrane, to cause cytotoxicity. This is supported by prior studies demonstrating the ability of perfluorinated amphiphiles to insert into hydrocarbon lipid bilayers and phase-separate into fluorine-rich microdomains. $^{54-56}$ A similar binary toxicity behavior was observed during hemolysis assays (Figure 4B). Both 20 and 30 mM PFNA-PFO $_{\rm c}$ emulsions were nonhemolytic at intermediate particle concentrations ($\leq \! 10^{5}$ particles/mL) but potently lysed erythrocytes at high particle densities. This hemolytic activity occurred without the acoustic trigger, indicating that, just like toxicity toward HUVEC cells, particle vaporization did not drive the off-target effects observed.

Based on these results, 10⁵ particle/mL concentrations of PFNA-PFO_c emulsions were employed for follow-up clotting time assays using platelet-rich plasma (PRP). Results in Figure 4C demonstrate that, in the absence of emulsions, exposure of PRP to US at a power of 2.0 W/cm² (50% DC, 30 s) is sufficient to cause a >2-fold reduction in the *in vitro* coagulation time (see water in Figure 4C, black bars). This is likely due to the ability of low-intensity US to mechanically stimulate platelet aggregation and promote thrombin generation. ^{51,57,58} The addition of PFNA-PFO_c droplets led to a slight reduction in the US-induced clotting time relative to

nonparticle-treated controls. For example, 20 mM PFNA-PFO_c emulsions reduced the coagulation time by an additional $\sim\!10\%$ relative to US treatment alone. This enhancement may come from the ability of these acoustic contrast agents to focus ultrasonic signals and enhance local thermal effects, 59 as well as activate platelets through shear forces generated during inertial bubble cavitation. 60

To mechanistically test this assertion, platelet activation was next investigated for 20 and 30 mM PFNA-PFO_c emulsions through flow cytometry analysis. In these experiments, bovine platelets were incubated with each particle formulation for 15 min before exposure to US (2.0 W/cm², 50% DC, 30 s). Treated platelets were then analyzed by flow cytometry, where platelet activation was monitored by the appearance of cellular aggregates that cause high forward scattering intensities. Results in Figure 4D show that exposure of platelets to the US alone was not sufficient to generate cellular aggregates relative to uninsonated control samples. However, treatment with both 20 and 30 mM PFNA-PFO_c emulsions caused platelet activation that generated highly scattering cellular agglomerates (see black arrows in Figure 4D), which were the greatest for the 20 mM formulation. Cavitation of the emulsions under US produced a slight, but discernable, increase in the number of activated platelets for both formulations. Taken together with results from our coagulation assays (Figure 4C), these findings suggest that, while US exposure alone is sufficient to induce significant coagulation, acoustic cavitation of 20 mM PFNA-PFO_c emulsions can activate platelets to further enhance clotting kinetics. This coagulation enhancement is less potent for 30 mM formulations, likely due to their lower US cavitation efficiency compared to 20 mM PFNA-PFO_c emulsions (Figure 3C). One explanation for this emulsion-mediated platelet activation may be due to the ability of fluoroalkyl surfactants to accumulate within platelet plasma membranes. 61 For example, perfluorooctanoic acid shows dose-dependent changes in the fluidity of platelet membranes, which in turn leads to increased calcium uptake and altered signaling pathways that regulate activation.6

In the second series of experiments, we exploit the ability of PFNA-PFO_c emulsions to be orthogonally activated under different conditions of US to enable programmable release of bioactive cargo to mammalian cells. As exemplary payloads, the lipophilic fluorophores DiO and DiI were dissolved in the PFO_c solvent before emulsification with 20 or 30 mM PFNA to create emulsions that cavitate at low and intermediate US powers, respectively. Preliminary ex cellulo experiments confirm that DiO- (20 mM PFNA) and DiI-loaded (30 mM PFNA) PFO_c emulsions can be acoustically activated in a sequential fashion at different powers of US (Figure S5). When applied to human A549 lung epithelial cells, both emulsions accumulated at the periphery of cells and remained intact prior to acoustic activation (Figure 5A, see 0 W/cm²). As designed, selective vaporization of DiO-loaded emulsions and preferential release of the fluorophore payload was achieved at low acoustic powers (0.4 W/cm²) without significant disruption of the orthogonal DiI-loaded droplets (Figure 5B). Increasing the US power to 2.0 W/cm² resulted in activation and fluorophore delivery from both formulations, as indicated by the incorporation of both dyes into the membranes of treated cells.

Next, we used confocal microscopy to investigate the ability to spatially control cargo delivery via US-mediated activation of DiI-loaded PFNA-PFO_c emulsions. Fluorescence images

collected at different positions along the treated A549 cell monolayer demonstrate robust DiI delivery to cells directly underneath the center of the US transducer (Figure 5C, left). A549 cells at the edge of the acoustic path receive collateral DiI delivery (Figure 5C, middle), while cells outside the acoustic field were minimally stained (Figure 5C, right). Magnified images shown in Figure 5D demonstrate that DiIloaded PFNA-PFO_c emulsions (red) remain intact at the monolayer region outside of the US field. Collectively, these results demonstrate the ability of PFNA-stabilized emulsions to provide orthogonal delivery of bioactive payloads in a US-guided, spatiotemporal manner.

CONCLUSIONS

In this study, we investigate how organofluorine emulsifiers alter the thermodynamic properties of PFC droplets by assembling in the inhomogeneous region of the fluorouswater interphase. We identify perfluorononanoic acid (PFNA) as a privileged amphiphile capable of modulating the interfacial Gibbs free energy of single-species PFC droplets. Complementary work by the Borden group has yielded mixed-phase systems in which the vaporization temperature of fluorous droplets can be altered through the incorporation of a solid fluorocarbon inner disc or "endoskeleton." Here, melting of the inner skeletal material, and its mixing with the emulsified phase, enhances or disrupts the cohesive intermolecular forces of the bulk liquid to control its phase transition temperature. As an alternative strategy, here, we manipulate the cohesive properties of only the fluorous droplet surface, instead of altering the behavior of the bulk liquid, to modulate the thermodynamic properties of the emulsion vehicle. This allows for the facile and scalable synthesis of single-phase, cargoloaded fluorous microdroplets that possess programmable acoustic behaviors. This property was subsequently exploited in two different biomedical contexts. First, we leverage the ability of PFNA-PFO_c emulsions to be acoustically vaporized at varied US powers to alter the kinetics of blood coagulation without generating significant off-target hemolysis or endothelial cell toxicity. A second example delivering lipophilic biosensors to mammalian cells served to demonstrate how interfacial tension of PFC emulsions can be modulated to achieve orthogonal delivery of bioactive payloads in a USguided, spatiotemporal manner. Collectively, these findings provide important insight into the thermodynamic modularity of PFC emulsions stabilized by chemically tractable fluoroalkyl emulsifiers. Continued advancement of these technologies may open new opportunities to develop stimuli-responsive PFC biomaterials and imaging-guided biomedical tools.

ASSOCIATED CONTENT

Supporting Information

The Supporting Information is available free of charge at https://pubs.acs.org/doi/10.1021/acsami.0c20352.

Emulsion particle counting, micrograph of PFO_c emulsion turbidity before and after US exposure, relationship between PFC bulk boiling point and EP₅₀ of emulsions, ζ -potential measurements of PFO_c emulsions before and after vaporization, and orthogonal US activation of dye-loaded PFNA-PFO_c emulsions and fluorophore delivery to A549 cells (PDF)

AUTHOR INFORMATION

Corresponding Author

Scott H. Medina — Department of Biomedical Engineering, Penn State University, University Park, Pennsylvania 16802, United States; Huck Institutes of the Life Sciences, Penn State University, University Park, Pennsylvania 16802, United States; orcid.org/0000-0001-5441-2164; Phone: 814-863-4758; Email: shm126@psu.edu

Authors

- Atip Lawanprasert Department of Biomedical Engineering, Penn State University, University Park, Pennsylvania 16802, United States
- Alda Chau Department of Biomedical Engineering, Penn State University, University Park, Pennsylvania 16802, United States
- Janna N. Sloand Department of Biomedical Engineering, Penn State University, University Park, Pennsylvania 16802, United States
- Sean Hannifin Department of Biomedical Engineering, Penn State University, University Park, Pennsylvania 16802, United States; Immunology Graduate Program, University of Michigan, Ann Arbor, Michigan 48109, United States

Complete contact information is available at: https://pubs.acs.org/10.1021/acsami.0c20352

Notes

The authors declare no competing financial interest.

ACKNOWLEDGMENTS

We acknowledge and thank the Penn State Microscopy and Cytometry Facility—University Park, PA for assistance with confocal microscopy. We also acknowledge the Penn State Materials Characterization Laboratory—University Park, PA for use of dynamic light scattering and pendant drop instrumentation. Funding for this research was provided by the NSF Faculty Early Career Development Program (CAREER) to S.H.M. under award number DMR-1845053. Funds from the Penn State Graduate Research Fellowship supported J.N.S.

REFERENCES

- (1) Kaewsaneha, C.; Tangboriboonrat, P.; Polpanich, D.; Eissa, M.; Elaissari, A. Janus Colloidal Particles: Preparation, Properties, and Biomedical Applications. ACS Appl. Mater. Interfaces 2013, 5, 1857–1869.
- (2) Sletten, E. M.; Swager, T. M. Readily Accessible Multifunctional Fluorous Emulsions. *Chem. Sci.* **2016**, *7*, 5091–5097.
- (3) Zarzar, L. D.; Sresht, V.; Sletten, E. M.; Kalow, J. A.; Blankschtein, D.; Swager, T. M. Dynamically Reconfigurable Complex Emulsions via Tunable Interfacial Tensions. *Nature* **2015**, *518*, 520–524.
- (4) Schmieder, A. H.; Caruthers, S. D.; Keupp, J.; Wickline, S. A.; Lanza, G. M. Recent Advances in ¹⁹Fluorine Magnetic Resonance Imaging with Perfluorocarbon Emulsions. *Engineering* **2015**, *1*, 475–489.
- (5) Srinivas, M.; Cruz, L. J.; Bonetto, F.; Heerschap, A.; Figdor, C. G.; De Vries, I. J. M. Customizable, Multi-Functional Fluorocarbon Nanoparticles for Quantitative In vivo Imaging using 19F MRI and Optical Imaging. *Biomaterials* **2010**, *31*, 7070–7077.
- (6) Lim, I.; Vian, A.; Van de Wouw, H. L.; Day, R. A.; Gomez, C.; Liu, Y.; Rheingold, A. L.; Campàs, O.; Sletten, E. M. Fluorous Soluble Cyanine Dyes for Visualizing Perfluorocarbons in Living Systems. *J. Am. Chem. Soc.* **2020**, *142*, 16072–16081.

- (7) Brambila, C. J.; Lux, J.; Mattrey, R. F.; Boyd, D.; Borden, M. A.; de Gracia Lux, C. Bubble Inflation Using Phase-Change Perfluor-ocarbon Nanodroplets as a Strategy for Enhanced Ultrasound Imaging and Therapy. *Langmuir* **2020**, *36*, 2954–2965.
- (8) Sheeran, P. S.; Matsuura, N.; Borden, M. A.; Williams, R.; Matsunaga, T. O.; Burns, P. N.; Dayton, P. A. Methods of Generating Submicrometer Phase-Shift Perfluorocarbon Droplets for Applications in Medical Ultrasonography. *IEEE Trans. Ultrason., Ferroelect., Freq. Contr.* 2017, 64, 252–263.
- (9) Martz, T. D.; Sheeran, P. S.; Bardin, D.; Lee, A. P.; Dayton, P. A. Precision Manufacture of Phase-Change Perfluorocarbon Droplets using Microfluidics. *Ultrasound Med. Biol.* **2011**, *37*, 1952–1957.
- (10) Duncanson, W. J.; Arriaga, L. R.; Ung, W. L.; Kopechek, J. A.; Porter, T. M.; Weitz, D. A. Microfluidic Fabrication of Perfluorohexane-Shelled Double Emulsions for Controlled Loading and Acoustic-Triggered Release of Hydrophilic Agents. *Langmuir* **2014**, *30*, 13765—13770
- (11) Centner, C. S.; Priddy, M. C.; Kopechek, J. A. Standing Acoustic Waves in Microfluidic Channels for Enhanced Intracellular Delivery of Molecular Compounds. *J. Acoust. Soc. Am.* **2019**, *145*, No. 1894.
- (12) Martz, T. D.; Bardin, D.; Sheeran, P. S.; Lee, A. P.; Dayton, P. A. Microfluidic Generation of Acoustically Active Nanodroplets. *Small* **2012**, *8*, 1876–1879.
- (13) Delgado, M.; Lázaro, A.; Mazo, J.; Zalba, B. Review on Phase Change Material Emulsions and Microencapsulated Phase Change Material Slurries: Materials, Heat Transfer Studies and Applications. *Renewable Sustainable Energy Rev.* **2012**, *16*, 253–273.
- (14) Wang, F.; Zhang, C.; Liu, J.; Fang, X.; Zhang, Z. Highly Stable Graphite Nanoparticle-Dispersed Phase Change Emulsions with Little Supercooling and High Thermal Conductivity for Cold Energy Storage. *Appl. Energy* **2017**, *188*, 97–106.
- (15) Hou, J.; Cao, T.; Idrees, F.; Cao, C. A Co-Sol-Emulsion-Gel Synthesis of Tunable and Uniform Hollow Carbon Nanospheres with Interconnected Mesoporous Shells. *Nanoscale* **2016**, *8*, 451–457.
- (16) Chen, J.; Zhang, P. Preparation and Characterization of Nano-Sized Phase Change Emulsions as Thermal Energy Storage and Transport Media. *Appl. Energy* **2017**, *190*, 868–879.
- (17) Rapoport, N. Phase-Shift, Stimuli-Responsive Perfluorocarbon Nanodroplets for Drug Delivery to Cancer. Wiley Interdiscip. Rev.: Nanomed. Nanobiotechnol. 2012, 4, 492–510.
- (18) Sloand, J. N.; Nguyen, T. T.; Zinck, S. A.; Cook, E. C.; Zimudzi, T. J.; Showalter, S. A.; Glick, A. B.; Simon, J. C.; Medina, S. H. Ultrasound-Guided Cytosolic Protein Delivery via Transient Fluorous Masks. *ACS Nano* **2020**, *14*, 4061–4073.
- (19) Fabiilli, M. L.; Lee, J. A.; Kripfgans, O. D.; Carson, P. L.; Fowlkes, J. B. Delivery of Water-Soluble Drugs using Acoustically Triggered Perfluorocarbon Double Emulsions. *Pharm. Res.* **2010**, 27, 2753–2765.
- (20) Javadi, M.; Pitt, W. G.; Tracy, C. M.; Barrow, J. R.; Willardson, B. M.; Hartley, J. M.; Tsosie, N. H. Ultrasonic Gene and Drug Delivery using eLiposomes. *J. Controlled Release* **2013**, *167*, 92–100. (21) Day, R. A.; Estabrook, D. A.; Logan, J. K.; Sletten, E. M.
- Fluorous Photosensitizers Enhance Photodynamic Therapy with Perfluorocarbon Nanoemulsions. *Chem. Commun.* **2017**, *53*, 13043–13046.
- (22) Estabrook, D. A.; Ennis, A. F.; Day, R. A.; Sletten, E. M. Controlling Nanoemulsion Surface Chemistry with poly(2-oxazoline) Amphiphiles. *Chem. Sci.* **2019**, *10*, 3994–4003.
- (23) Day, R. A.; Estabrook, D. A.; Wu, C.; Chapman, J. O.; Togle, A. J.; Sletten, E. M. Systematic Study of Perfluorocarbon Nanoemulsions Stabilized by Polymer Amphiphiles. *ACS Appl. Mater. Interfaces* **2020**, *12*, 38887–38898.
- (24) Huang, J.; Xu, J. S.; Xu, R. X. Heat-Sensitive Microbubbles for Intraoperative Assessment of Cancer Ablation Margins. *Biomaterials* **2010**, *31*, 1278–1286.
- (25) Strohm, E.; Rui, M.; Gorelikov, I.; Matsuura, N.; Kolios, M. Vaporization of Perfluorocarbon Droplets using Optical Irradiation. *Biomed. Opt. Express* **2011**, *2*, 1432–1442.

- (26) Yuan, Z.; Demith, A.; Stoffel, R.; Zhang, Z.; Park, Y. C. Light-Activated Doxorubicin-Encapsulated Perfluorocarbon Nanodroplets for On-Demand Drug Delivery In an In Vitro Angiogenesis Model: Comparison Between Perfluoropentane and Perfluorohexane. *Colloids Surf., B* 2019, 184, No. 110484.
- (27) Luke, G. P.; Hannah, A. S.; Emelianov, S. Y. Super-Resolution Ultrasound Imaging in Vivo with Transient Laser-Activated Nanodroplets. *Nano Lett.* **2016**, *16*, 2556–2559.
- (28) Zhu, H.; Qin, D.; Wu, Y.; Jing, B.; Liu, J.; Hazlewood, D.; Zhang, H.; Feng, Y.; Yang, X.; Wan, M.; Wu, D. Laser-Activated Bioprobes with High Photothermal Conversion Efficiency for Sensitive Photoacoustic/Ultrasound Imaging and Photothermal Sensing. ACS Appl. Mater. Interfaces 2018, 10, 29251–29259.
- (29) Hannah, A.; Luke, G.; Wilson, K.; Homan, K.; Emelianov, S. Indocyanine Green-Loaded Photoacoustic Nanodroplets: Dual Contrast Nanoconstructs for Enhanced Photoacoustic and Ultrasound Imaging. ACS Nano 2014, 8, 250–259.
- (30) Deng, L.; Cai, X.; Sheng, D.; Yang, Y.; Strohm, E. M.; Wang, Z.; Ran, H.; Wang, D.; Zheng, Y.; Li, P.; et al. A Laser-Activated Biocompatible Theranostic Nanoagent for Targeted Multimodal Imaging and Photothermal Therapy. *Theranostics* **2017**, *7*, 4410–4423.
- (31) Reznik, N.; Williams, R.; Burns, P. N. Investigation of Vaporized Submicron Perfluorocarbon Droplets as an Ultrasound Contrast Agent. *Ultrasound Med. Biol.* **2011**, *37*, 1271–1279.
- (32) Matsunaga, T. O.; Sheeran, P. S.; Luois, S.; Streeter, J. E.; Mullin, L. B.; Banerjee, B.; Dayton, P. A. Phase-Change Nanoparticles Using Highly Volatile Perfluorocarbons: Toward a Platform for Extravascular Ultrasound Imaging. *Theranostics* **2012**, *2*, 1185–1198.
- (33) Sheeran, P. S.; Luois, S. H.; Mullin, L. B.; Matsunaga, T. O.; Dayton, P. A. Design of Ultrasonically-Activatable Nanoparticles Using Low Boiling Point Perfluorocarbons. *Biomaterials* **2012**, 33, 3262–3269.
- (34) Kagan, D.; Benchimol, M. J.; Claussen, J. C.; Chuluun-Erdene, E.; Esener, S.; Wang, J. Acoustic Droplet Vaporization and Propulsion of Perfluorocarbon-Loaded Microbullets for Targeted Tissue Penetration and Deformation. *Angew. Chem., Int. Ed.* **2012**, *51*, 7519–7522.
- (35) Sheeran, P. S.; Dayton, P. A. Phase-Change Contrast Agents for Imaging and Therapy. *Curr. Pharm. Des.* **2012**, *18*, 2152–2165.
- (36) Shakya, G.; Hoff, S. E.; Wang, S.; Heinz, H.; Ding, X.; Borden, M. A. Vaporizable Endoskeletal Droplets via Tunable Interfacial Melting Transitions. *Sci. Adv.* **2020**, *6*, No. eaaz7188.
- (37) Rojas, J. D.; Dayton, P. A. Optimizing Acoustic Activation of Phase Change Contrast Agents With the Activation Pressure Matching Method: A Review. *IEEE Trans. Ultrason., Ferroelect., Freq. Contr.* **2017**, *64*, 264–272.
- (38) Sheeran, P. S.; Dayton, P. A. Improving the Performance of Phase-Change Perfluorocarbon Droplets for Medical Ultrasonography: Current Progress, Challenges, and Prospects. *Scientifica* **2014**, 2014, No. 579684.
- (39) Fan, Z.; Kumon, R. E.; Deng, C. X. Mechanisms of Microbubble-Facilitated Sonoporation for Drug and Gene Delivery. *Ther. Delivery* **2014**, *5*, 467–486.
- (40) Rapoport, N. Drug-Loaded Perfluorocarbon Nanodroplets for Ultrasound-Mediated Drug Delivery. In *Therapeutic Ultrasound*; Springer, 2016; pp 221–241.
- (41) Kawabata, K.-i.; Sugita, N.; Yoshikawa, H.; Azuma, T.; Umemura, S.-i. Nanoparticles with Multiple Perfluorocarbons for Controllable Ultrasonically Induced Phase Shifting. *Jpn. J. Appl. Phys.* **2005**, *44*, No. 4548.
- (42) Riess, J. G.; Krafft, M. P. Fluorocarbon Emulsions as In Vivo Oxygen Delivery Systems: Background and Chemistry. In *Blood Substitutes*; Elsevier, 2006; pp 259–275.
- (43) Patist, A.; Chhabra, V.; Pagidipati, R.; Shah, R.; Shah, D. Effect of Chain Length Compatibility on Micellar Stability in Sodium Dodecyl Sulfate/alkyltrimethylammonium Bromide Solutions. *Langmuir* 1997, 13, 432–434.

- (44) Medina, S. H.; Michie, M. S.; Miller, S. E.; Schnermann, M. J.; Schneider, J. P. Fluorous Phase-Directed Peptide Assembly Affords Nano-Peptisomes Capable of Ultrasound-Triggered Cellular Delivery. *Angew. Chem., Int. Ed.* **2017**, *56*, 11404–11408.
- (45) Freire, M. G.; Carvalho, P. J.; Queimada, A. J.; Marrucho, I. M.; Coutinho, J. A. P. Surface Tension of Liquid Fluorocompounds. *J. Chem. Eng. Data* **2006**, *51*, 1820–1824.
- (46) Brennen, C. E. Cavitation and Bubble Dynamics; Cambridge University Press, 2013.
- (47) Brennen, C. E. Fundamentals of Multiphase Flow; Cambridge University Press: Cambridge, 2005.
- (48) Leighton, T. The Acoustic Bubble; Academic Press, 2012.
- (49) Sheeran, P. S.; Dayton, P. A. Phase-Change Contrast Agents for Imaging and Therapy. *Curr. Pharm. Des.* **2012**, *18*, 2152–2165.
- (50) Guo, J.; Tian, G.; Zhao, Q.; Jiang, T. Fast Hemostasis: a Win-Win Strategy for Ultrasound and Microwave Ablation. *OncoTargets Ther.* **2018**, *11*, 1395–1402.
- (51) Nguyen, V. P.; Kim, J.; Ha, K.-l.; Oh, J.; Kang, H. W. Feasibility Study on Photoacoustic Guidance for High-Intensity Focused Ultrasound-Induced Hemostasis. *J. Biomed. Opt.* **2014**, *19*, No. 105010.
- (52) Zhao, D.-w.; Tian, M.; Yang, J.-z.; Du, P.; Bi, J.; Zhu, X.; Li, T. Hemostatic Mechanism Underlying Microbubble-Enhanced Non-Focused Ultrasound in the Treatment of a Rabbit Liver Trauma Model. *Exp. Biol. Med.* **2017**, *242*, 231–240.
- (53) Goertz, D. E. An Overview of the Influence of Therapeutic Ultrasound Exposures on the Vasculature: High Intensity Ultrasound and Microbubble-Mediated Bioeffects. *Int. J. Hyperthermia* **2015**, *31*, 134–144.
- (54) Pérez, F.; Nadal, M.; Navarro-Ortega, A.; Fàbrega, F.; Domingo, J. L.; Barceló, D.; Farré, M. Accumulation of Perfluoroalkyl Substances in Human Tissues. *Environ. Int.* **2013**, *59*, 354–362.
- (55) Naarmann, N.; Bilgiçer, B.; Meng, H.; Kumar, K.; Steinem, C. Fluorinated Interfaces Drive Self-Association of Transmembrane α Helices in Lipid Bilayers. *Angew. Chem., Int. Ed.* **2006**, 45, 2588–2591.
- (56) Bilgiçer, B.; Kumar, K. *De novo* Design of Defined Helical Bundles in Membrane Environments. *Proc. Natl. Acad. Sci. U. S. A.* **2004**, *101*, 15324–15329.
- (57) Poliachik, S. L.; Chandler, W. L.; Mourad, P. D.; Ollos, R. J.; Crum, L. A. Activation, Aggregation and Adhesion of Platelets Exposed to High-Intensity Focused Ultrasound. *Ultrasound Med. Biol.* **2001**, *27*, 1567–1576.
- (58) Stief, T. W.; Klingmüller, V.; Müller-Stüler, E. Thrombin Generation by Diagnostic Ultrasound. *Hemostasis Laboratory* **2011**, *4*, 335.
- (59) Umemura, S.-i.; Kawabata, K.-i.; Sasaki, K. Vivo Acceleration of Ultrasonic Tissue Heating by Microbubble Agent. *IIEEE Trans. Ultrason., Ferroelect., Freq. Contr.* **2005**, *52*, 1690–1698.
- (60) Poliachik, S. L.; Chandler, W. L.; Ollos, R. J.; Bailey, M. R.; Crum, L. A. The Relation Between Cavitation and Platelet Aggregation During Exposure to High-Intensity Focused Ultrasound. *Ultrasound Med. Biol.* **2004**, *30*, 261–269.
- (61) De Toni, L.; Radu, C. M.; Sabovic, I.; Di Nisio, A.; Dall'Acqua, S.; Guidolin, D.; Spampinato, S.; Campello, E.; Simioni, P.; Foresta, C. Increased Cardiovascular Risk Associated with Chemical Sensitivity to Perfluoro-Octanoic Acid: Role of Impaired Platelet Aggregation. *Int. J. Mol. Sci.* **2020**, *21*, No. 399.